Thermodynamic Modeling of Hydrothermal Synthesis of Ceramic Powders

Małgorzata M. Łencka and Richard E. Riman*

Department of Ceramics, College of Engineering, Rutgers, The State University of New Jersey, P.O. Box 909, Piscataway, New Jersey 08855-0909

Received August 24, 1992. Revised Manuscript Received October 16, 1992

A thermodynamic method is proposed for analyzing the hydrothermal synthesis of ceramic materials. The method utilizes standard-state thermodynamic data for solid and aqueous species and a comprehensive activity coefficients model to represent solution nonideality. The method is used to generate phase stability diagrams for the species that predominate in the system. The stability diagrams can be used to predict the optimum suspension synthesis conditions (i.e., feedstock composition, pH and temperature) for hydrothermal synthesis of ceramic materials. The synthesis of barium titanate ($BaTiO_3$(s)) and lead titanate ($PbTiO_3$(s)) are discussed as examples. In the case of the synthesis of $BaTiO_3$(s), which can be obtained at temperatures as low as 363 K, it is important to use solutions of appropriate pH. Practical techniques have been suggested to maintain the required pH by using a correct molar ratio of feedstocks, such as barium hydroxide ($Ba(OH)_2$(s)) to titanium dioxide (TiO_2(s)) or use of a mineralizer such as sodium hydroxide (NaOH(s)). It has been shown that contact with atmospheric carbon dioxide (CO_2(g)) will always lead to the contamination of the product with barium carbonate ($BaCO_3$(s)). Also, a low-temperature synthesis of $PbTiO_3$(s) has been proposed.

Introduction

Hydrothermal synthesis is a useful method for preparing myriad ceramic (e.g., ferroelectric and relaxor) materials from a variety of precursor feedstocks (e.g., oxides, nitrates, and alkoxides). The hydrothermal medium is attractive for ceramic powder synthesis because the combined effects of solvent, temperature, and pressure on ionic reaction equilibria can stabilize desirable products while inhibiting the formation of undesirable compounds. Also, hydrothermal synthesis makes it possible to prepare anhydrous ceramic powders in a single process step and does not require elaborate apparatus or expensive reagents.[1-5]

Hydrothermal synthesis involves reactions, mostly of ionic nature, between heterogeneous phases. The interaction between the solid and fluid phases determine the physical characteristics of the powder. Therefore, the powder properties can be controlled by utilizing chemical process variables such as temperature, pressure, reactant concentrations, pH, etc.[6] This requires the knowledge of stability diagrams for hydrothermal systems. The stability diagram shows the regions of reagent concentrations and pH for which various species predominate in the system. Thus, the stability diagrams indicate the optimum synthesis conditions for which the desirable products are thermodynamically stable.

Traditionally, the process variables, with few exceptions,[7-9] were adjusted empirically in a trial-and-error manner. Stability diagrams were considered for a limited number of hydrothermal systems by assuming that the aqueous solutions were ideal.[7,10] However, this is a crude approximation. It is especially inaccurate when concentrated electrolyte solutions are utilized or when a multitude of competing reactions occur in a solution, thus making the equilibrium concentrations of various species strongly dependent on activity coefficients.

In this work we propose a rigorous approach based on a realistic thermodynamic model of electrolyte solutions. This approach makes it possible to predict the optimum synthesis conditions (i.e., feedstock composition, pH, temperature, and pressure) to minimize the need for trial-end-error experimentation. Stability diagrams useful for the synthesis of $BaTiO_3$(s) and $PbTiO_3$(s) ceramic powders will be presented.

Thermodynamic Model

To establish a phase stability diagram, we need to compute equilibrium concentrations of each species in a system as a function of temperature, pressure, and the initial amount of reagents. Let us assume that we have k independent reactions. The jth reaction ($j = 1, ..., k$) involves n_j different chemical species $A_i^{(j)}$ ($i = 1, ..., n_j$). Thus, the system can be described by the following set of reactions:

$$\sum_{i=1}^{n_j} \nu_i^{(j)} A_i^{(j)} = 0 \qquad j = 1, ..., k \tag{1}$$

where $\nu_i^{(j)}$ is the stoichiometric number of species $A_i^{(j)}$.

(1) Riman, R. E. *Proceedings of the 11th Risø International Symposium on Metallurgy and Material Science: Structural Ceramics—Processing, Microstructure and Properties*; Bentzen, J. J., Bilde-Sørensen, J. B., Christiansen, N., Horsewell, A., Ralph, B., Eds.; Risø National Laboratory: Roskilde, Denmark, 1990; p 111.
(2) Dawson, W. J. *Ceram. Bull.* **1988**, *67*, 1673.
(3) Christensen, A. N. *Rev. Chim. Miner.* **1969**, *6*, 1187.
(4) Laudise, R. A. *Chem. Eng. News* **1987**, *28*, 30.
(5) Stambaugh, E. P.; Miller, J. F. *Proceedings of the First International Symposium on Hydrothermal Reactions*; Somiya, S., Ed.; Gakujutsu Bunken Fukyu-Kai: Tokyo, Japan, 1982; pp 859-872.
(6) Rabenau, A. *J. Mater. Educ.* **1988**, *10*, 543.
(7) Adair, J. H.; Denkiewicz, R. P.; Arriagada, F. J.; Osseo-Asare, K. *Ceramic Transactions, Ceramic Powder Science IIA*; Messing, G. L., Fuller Jr., E. R., Hausner, H., Eds.; American Ceramic Society: Westerville, OH, 1988; Vol. 1, 135.
(8) Fox, G. R.; Adair, J. H.; Newnham, R. E. *J. Mater. Sci.* **1990**, *25*, 3634.
(9) Utech, B. L. *The Effect of Solution Chemistry on Barium Titanate Ceramics*; The Pennsylvania State University: University Park, PA, 1990.

0897-4756/93/2805-0061$04.00/0

Complete information about the equilibrium state of each of these reactions is provided by the standard Gibbs energy change of the reaction:

$$\Delta G^\circ_{\mathrm{RXN},j} = \sum_{i=1}^{n_j} \nu_i^{(j)} G^\circ_f(A_i^{(j)}) = -RT \ln K_j(T,P) \qquad j = 1, ..., k \quad (2)$$

where $G^\circ_f(A_i^{(j)})$ is the standard Gibbs energy of formation of species $A_i^{(j)}$ and K_j is the equilibrium constant of reaction j.

In this work we use molality m as the concentration unit. Therefore, the equilibrium constant is expressed as

$$K_j(T,P) = \prod_{i=1}^{n_j} (m_{A_i^{(j)}} \gamma_{A_i^{(j)}})^{\nu_i^{(j)}} \qquad j = 1, ..., k \quad (3)$$

where $\gamma_{A_i^{(j)}}$ is the activity coefficient of species $A_i^{(j)}$.

In addition to k chemical equilibrium equations (eq 2) we have mass balance equations, whose number depends on the particular case, and an electroneutrality balance equation. This system of equations can be solved for equilibrium concentrations of reacting species provided that the standard Gibbs energies of formation and activity coefficients are known.

Standard-State Properties

To calculate the standard Gibbs energy of formation of each species at the temperature and pressure of interest, the values of the standard Gibbs energy ΔG°_f and enthalpy ΔH°_f of formation, and entropy S° at a reference temperature (usually 298.15 K) as well as partial molar volume V° and heat capacity C_p° as function of temperature are required. Subsequently, $G_f(T,P)$ is calculated using standard thermodynamic relations. In many cases, these data are available from existing compilations of thermochemical data. Whenever possible, the data should be taken from critically evaluated and consistent sources. Usually, the consistency of a data set can be checked by verifying the conformity of relations between experimental values of G, H, S, C_p, V, etc., to the general relations of thermodynamics. Also, the consistency of thermochemical data for a given substance can be determined by calculating the data on the basis of several reactions.

According to this criterion, the CODATA Key Values,[11] the compilations of NBS,[12] JANAF,[13] and Medvedev et al.[14] were preferred because they contain carefully selected and evaluated data. However, they do not contain data for many species of interest. Barin's[15] recent compilation is most complete and can be treated with confidence. Also, the data bank of Johnson et al.[16] was extensively used because their data were taken from consistent data sources and supplemented by estimates which were also checked for consistency.

In many cases no experimental data are available and predictive methods are necessary. This is frequently the case for ions, for which the Helgeson–Kirkham–Flowers (HKF) estimation method is very useful.[17-22] A software package[16] is also available that facilitates the application of the HKF equation.

Activity Coefficients

The activity coefficient model used in this work[23,24] is based on a combination of two models published by Bromley[25,26] and Pitzer.[27] The original method of Bromley is an extended Debye–Hückel[28] equation which can be used in a semipredictive mode because correlations have been established for its parameters. The Pitzer model is an extended Debye–Hückel equation with a virial-type expansion to account for short-range interactions. The Pitzer equation makes it possible to obtain a very good correlation of experimental data, but requires a significant amount of experimental input information for parameter regression. The combined model, developed by OLI Systems, Inc.,[24] utilizes an Debye–Hückel term for long-range ion–ion interactions, a modified Bromley expression (Bromley–Zemaitis) for short-range ion–ion interactions and the Pitzer expression for ion–neutral molecule interactions. The Pitzer term is used in a simplified version without taking into account three-body interactions.

The activity coefficient for an ion i is

$$\log \gamma_i = \mathrm{DH}_i + \mathrm{BZ}_i + P_i \quad (4)$$

where DH_i is the Debye–Hückel term defined as

$$\mathrm{DH}_i = \frac{-A|z_i|^2 I^{1/2}}{1 + I^{1/2}} \quad (5)$$

where A is the Debye–Hückel coefficient that depends on temperature and solvent properties,[23] z_i is the number of charges on ion i, m_i is the molality of species i, I is the ionic

(10) Osseo-Asare, K.; Arriagada, F. J.; Adair, J. H. *Ceramic Transaction, Ceramic Powder Science IIA*; Messing, G. L., Fuller Jr., E. R., Hausner, H., Eds.; American Ceramic Society: Westerville, OH, 1988; Vol. 1, p 47.

(11) CODATA Recommended Key Values for Chemical Thermodynamic Properties; CODATA Special Report, No. 3 (1975), No. 8 (1980), CODATA Bulletin No. 10 (1973), No. 28 (1978); CODATA, Paris.

(12) (a) Wagman, D. D.; Evans, W. H.; Parker, W. B.; Halow, I.; Bailey, S. M.; Schumm, R. H. *Selected Values of Chemical Thermodynamic Properties*; NBS Technical Note 270/3-8, 1968–1982. (b) Wagman, D. D.; Evans, W. H.; Parker, W. B.; Schumm, R. H.; Halow, I.; Bailey, S. M.; Churney, K. L.; Nuttall, R. L. The NBS Tables of Chemical Thermodynamic Properties. *J. Phys. Chem. Ref. Data* **1982**, *11*, Suppl. No. 2.

(13) (a) Stull, D. R.; Prophet, H. *JANAF Thermochemical Tables*, 2nd ed.; NSRDS-NBS 37; U.S. Government Printing Office: Washington, DC, 1971. (b) Chase, M. W., Jr.; Davies, C. A.; Downey, J. R., Jr.; Frurip, D. J.; McDonald, R. A.; Syverud, A. N. JANAF Thermochemical Tables, 3rd ed. *J. Phys. Chem. Ref. Data* 1985, *14*, Suppl. No. 1.

(14) Medvedev, V. A.; Bergman, G. A.; Gurvich, L. V.; Yungman, V. S.; Vorobiev, A. F.; Kolesov, V. P. *Thermal Constants of Substances*; Glushko, V. P., Ed.; VINITII: Moscow, 1965–1982; Vol. 1–10.

(15) Barin, I. In collaboration with Sauert, F.; Schultze-Rhonhof, E.; Shu Sheng, W. *Thermochemical Data of Pure Substances*; VCH Publishers: Weinheim, 1989.

(16) Johnson, J. W.; Oelkers, E. H.; Helgeson, H. C. *SUPCRT 92: A Software Package for Calculating the Standard Molal Thermodynamic Properties of Minerals, Gases, Aqueous Species, and Reactions from 1-5000 bars and 0 to 1000 °C*; University of California, Berkeley and Lawrence Livermore National Laboratory: Berkeley, 1991.

(17) Helgeson, H. C. *J. Phys. Chem.* **1967**, *71*, 3121.

(18) Helgeson, H. C. *Am. J. Sci.* **1969**, *267*, 729.

(19) Helgeson, H. C.; Kirkham D. H. *Am. J. Sci.* **1976**, *276*, 97.

(20) Helgeson, H. C.; Kirkham, D. H.; Flowers, G. C. *Am. J. Sci.* **1981**, *281*, 1249.

(21) Shock, E. L.; Helgeson, H. C. *Geochim. Cosmochim. Acta* **1988**, *52*, 2009.

(22) Shock, E. L.; Helgeson, H. C.; Sverjensky, D. A. *Geochim. Cosmochim. Acta* **1989**, *53*, 2157.

(23) Zemaitis, J. F., Jr.; Clark, D. M.; Rafal, M.; Scrivner, N. C. *Handbook of Aqueous Electrolyte Thermodynamics: Theory & Application*; American Institute of Chemical Engineers, Inc.: New York, 1986.

(24) Rafal, M. International Conference on Thermodynamics of Aqueous Systems with Industrial Applications: Virginia, 1987.

(25) Bromley, L. A. *AIChE J.* **1973**, *19*, 313.

(26) Bromley, L. A. *AIChE J.* **1974**, *20*, 326.

(27) Pitzer, K. S. *J. Phys. Chem.* **1973**, *77*, 268.

(28) Debye, P.; Hückel, E. *Phys. Z.* **1923**, *24*, 185.

strength:

$$I = 0.5\sum_i z_i^2 m_i \quad (6)$$

BZ_i is the Bromley–Zemaitis term for ion–ion interactions:

$$BZ_i = \sum_{j=1}^{NO}\left[\frac{|z_i| + |z_i|}{2}\right]^2 \beta_{ij} m_j \quad (7)$$

$$\beta_{ij} = \frac{(0.06 + 0.6B_{ij})|z_i z_j|}{(1 + 1.5I/|z_i z_j|)^2} + B_{ij} + C_{ij}I + D_{ij}I^2 \quad (8)$$

where NO is the number of ions with charge opposite to that of the ion being represented, and B_{ij}, C_{ij}, and D_{ij} are temperature-dependent parameters for cation–anion interactions.

Finally, the Pitzer term P_i for ion–neutral molecule interactions is

$$P_i = \sum_{j=1}^{NM} BP_{ij} m_j + \frac{z_i^2}{4I^2} BPS_j \quad (9)$$

$$BP_{ij} = \beta_{ij}^{(0)} + \beta_{ij}^{(1)} + (1 + 2I^{1/2})[1 - \exp(-2I^{1/2})]/2I \quad (10)$$

$$BPS_j = 0.86859 m_j \sum_{k=1}^{NS} BPP_{jk} m_k \quad (11)$$

$$BPP_{jk} = \beta_{jk}^{(1)}[1 - (1 + 2I^{1/2} + 2I)\exp(-2I^{1/2})] \quad (12)$$

where NM is the number of molecular species in solution, NS is the number of species in solution, and $\beta_{ij}^{(0)}$ and $\beta_{ij}^{(1)}$ are temperature-dependent parameters for each ion–molecule and molecule–molecule interaction.

The activity coefficients of non-ionic molecules other than water involve only the Pitzer term:

$$\log \gamma_i = 2\sum_{j=1}^{NS} BP_{ij} m_i \quad (13)$$

The solvent (water) activity is obtained from the above expressions and the Gibbs–Duhem equation:

$$\log a_{H_2O} = \frac{1}{\sum_{i=1}^{NC} z_i^2 m_i \sum_{j=1}^{NA} z_j^2 m_j} \sum_{i=1}^{NC}\sum_{j=1}^{NA} |z_i z_j| \beta_{ij} m_i m_j - 0.01801 \sum_{i=1}^{NM}\left[m_i + 2\sum_{j=1}^{NS} BPW_{ij} m_i m_j\right] \quad (14)$$

where NC and NA are the numbers of cations and anions in solution, respectively.

Equations 4–14 determine the activity coefficients in a multicomponent aqueous solution containing both ionic and neutral species. These equations, coupled with standard-state thermodynamic data, can be used to solve eqs 2 and 3 and material and electroneutrality balances. The OLI Systems software[29] was used for this purpose.

To verify the OLI model, activity coefficients have been calculated for $BaCl_2$(aq), NaOH(aq) and $Pb(NO_3)_2$(aq), and compared with experimental data in Table I. These electrolytes have been chosen because they contain ions that are of interest in our investigation of hydrothermal systems. As shown in Table I, the relative deviations between calculated and experimental activity coefficients lie between 2.7 and 6.9% for NaOH(aq), 0.2 and 1.0% for $BaCl_2$(aq), and 1.7–3.9% for $Pb(NO_3)_2$(aq). This accuracy is adequate for the computation of reaction equilibria.

(29) OLI Prochem Software V9.0; OLI Systems, Inc.: Morris Plains, NJ, 1992.

Table I. Comparison of Activity Coefficients Calculated from the OLI Model with Experimental Data[57]

	NaOH(aq)		$BaCl_2$(aq)		$Pb(NO_3)_2$(aq)	
m	γ^{exp}[a]	γ^{calc}[b]	γ^{exp}	γ^{calc}	γ^{exp}	γ^{calc}
0.1	0.766	0.787	0.500	0.499	0.395	0.402
0.3	0.708	0.734	0.419	0.420	0.260	0.271
0.5	0.690	0.720	0.397	0.396	0.205	0.213
0.7	0.681	0.718	0.391	0.388	0.172	0.179
1.0	0.678	0.728	0.395	0.391	0.141	0.145

[a] γ^{exp}: experimental activity coefficients.[57] [b] γ^{calc}: calculated activity coefficients.

Table II. Relevant Equilibria in the Ba–Ti and Pb–Ti Hydrothermal Systems

1. $H_2O = H^+ + OH^-$
2. $H_2O(g) = H_2O$
3. $TiO_2(s) + OH^- = HTiO_3^-$
4. $Ba(OH)_2(s) = Ba^{2+} + 2OH^-$
5. $BaOH^+ = Ba^{2+} + OH^-$
6. $BaTiO_3(s) + H_2O = Ba^{2+} + 2OH^- + TiO_2(s)$
7. $Ba(OH)_2{\cdot}8H_2O(s) = Ba^{2+} + 2OH^- + 8H_2O$
8. $BaO(s) + 2H^+ = Ba^{2+} + H_2O$
9. $Ba_2TiO_4(s) + 2H_2O = 2Ba^{2+} + 4OH^- + TiO_2(s)$
10. $CO_2(g) = CO_2(aq)$
11. $CO_2(aq) + H_2O = H^+ + HCO_3^-$
12. $HCO_3^- = H^+ + CO_3^{2-}$
13. $BaCO_3(s) = Ba^{2+} + CO_3^{2-}$
14. $BaCO_3(aq) = Ba^{2+} + CO_3^{2-}$
15. $BaHCO_3^+ = Ba^{2+} + HCO_3^-$
16. $Ti^{4+} + H_2O = TiOH^{3+} + H^+$
17. $TiOH^{3+} + H_2O = Ti(OH)_2^{2+} + H^+$
18. $Ti(OH)_2^{2+} + H_2O = Ti(OH)_3^+ + H^+$
19. $Ti(OH)_3^+ + H_2O = Ti(OH)_4(aq) + H^+$
20. $Ti(OH)_4(aq) = TiO_2(s) + 2H_2O$
21. $PbO(s) + H_2O = Pb^{2+} + 2OH^-$
22. $PbO(aq) + H_2O = PbOH^+ + OH^-$
23. $PbOH^+ = Pb^{2+} + OH^-$
24. $Pb(OH)_2(s) = Pb^{2+} + 2OH^-$
25. $Pb^{2+} + 2OH^- = H^+ + HPbO_2^-$
26. $Pb_2OH^{3+} + H^+ = 2Pb^{2+} + H_2O$
27. $Pb_3(OH)_4^{2+} = 3Pb^{2+} + 4OH^-$
28. $Pb_4(OH)_4^{4+} = 4Pb^{2+} + 4OH^-$
29. $Pb_6(OH)_8^{4+} = 6Pb^{2+} + 8OH^-$
30. $PbTiO_3(s) + H_2O = Pb^{2+} + 2OH^- + TiO_2(s)$

Our calculations made it possible to construct stability diagrams that indicate which species dominate in the investigated system. The stability diagrams show predominance fields for several species as functions of pH and total molality of reactant species in the solution at constant temperature. Total molality and pH were chosen as independent variables because they are easily measurable and can be used in practice to determine the desired compositions of feedstocks for hydrothermal synthesis. Boundaries between the predominance fields of different aqueous species denote the loci where both species have equal concentrations. Boundaries between solid and aqueous species correspond to the beginning of precipitation (or, alternatively, complete disappearance) of the solid phase. In practice, an equilibrium point was assumed to lie on the solid–aqueous species boundary when less than 0.25% of the feedstock was found to be in the form of a solid phase.

Results

Synthesis of $BaTiO_3$(s). $BaTiO_3$(s) has been chosen as an example because its synthesis conditions have been experimentally determined[30–36] and, on the other hand, standard-state thermodynamic properties are known for

all reactants involved in the synthesis. Therefore, the computed results for the synthesis of $BaTiO_3$(s) can be verified by comparing them with experimentally determined conditions.

All possible reactions that may occur in the hydrothermal medium are summarized in Table II. The standard thermodynamic properties of species for these reactions are listed in Table III. For H^+ all standard state properties are, by convention, equal to zero. For OH^- and H_2O the critically evaluated values from the CODATA[11] compilation were used. In the case of $Ba(OH)_2$(s), the data from the compilations of Barin[15] and Medvedev et al.[14] are in reasonable agreement and the differences between them do not affect the results of calculations. The Medvedev et al. data were adopted in the calculations. Similarly, there are small differences between the data for BaO(s)[12-15,44] and Ba_2TiO_4(s).[15,37] However, these species are practically insignificant, and the selection of the data for them is not important. Some small differences between data sets were noted for TiO_2(s)[12-16,44] for both the rutile and anatase forms. In this case the values from Johnson et al. data bank[16] have been used because they form a part of a large, critically evaluated compilation. Results of calculations have been found to be insensitive to choosing rutile and anatase and, therefore, only the data for rutile have been used. $BaTiO_3$(s) is the only compound in the system for which significant discrepancies in standard state data exist between those given by Barin[15] and Naumov et al.[37] While the Naumov et al. compilation provides data recommended on the basis of literature comparisons, their consistency does not appear to have been checked. Barin's[15] data were adopted for $BaTiO_3$(s). Among the hydrates of barium hydroxide, $Ba(OH)_2 \cdot 8H_2O$(s) is the most stable, and it was not necessary to explicitly take into account other less stable hydrates. For $Ba(OH)_2 \cdot 8H_2O$(s), the only available data are those from Medvedev et al.[14]

The most abundant, although not complete, source of information for ions is the Johnson et al.[16] data bank. For ions that were not included into this bank, the data were taken from the Medvedev et al.[14] compilation. Experimental data for ions, especially more complex ones (Ti^{4+}, $TiOH^{3+}$, $Ti(OH)_2^{2+}$, $Ti(OH)_3^+$), are much more scarce and usually limited to the Gibbs energies at 298.15 K. These values were taken from Medvedev et al.[14] compilation. For some ions (Ti^{4+}, $HTiO_3^-$) entropies are also available.[21,38] However, there is a general lack of data for hydroxy complexes of titanium. In this case the entropies have been estimated using a technique proposed by Baes and Mesmer.[39]

Following Baes and Mesmer, the entropy of the reaction

$$Ti^{4+} + H_2O = Ti(OH)^{3+} + H^+ \quad (15)$$

is given by

$$\Delta S_{15} = 1.772 \log K_{15} + 19.12(z/d) \quad (16)$$

where K_{15} is the equilibrium constant of this reaction at 298.15 K, z is the cation charge (+4 in this case), and d is the distance between the metal and oxygen (Ti–O). The quantity (z/d) is estimated from

$$\ln K_{15} = A + 11.0(z/d) \quad (17)$$

where A is assigned a characteristic value for several groups of cations. For Ti^{4+}, the value of −19.1 is recommended. Since the entropies of Ti^{4+} and water are known,[11,21] the entropy of the $Ti(OH)^{3+}$ cation can be calculated from

$$S^\circ[Ti(OH)_3^+] = \Delta S_{15} + S^\circ(Ti^{4+}) + S^\circ(H_2O) \quad (18)$$

A similar technique is employed for further hydrolysis reactions:

$$Ti(OH)_y^{(4-y)+} + H_2O = Ti(OH)_{y+1}^{(4-y-1)+} + H^+ \quad (19)$$

In this case the entropy of reaction is

$$\Delta S_{19} = -17.8 + 12.2(z - y) \quad (20)$$

where $z = 4$ for titanium ion. The entropy of the $Ti(OH)_{y+1}^{(4-y-1)+}$ ion is then given by

$$S^\circ[Ti(OH)_{y+1}^{(4-y-1)+}] = \Delta S_{19} + S^\circ[Ti(OH)_y^{(4-y)+}] + S^\circ(H_2O) \quad (21)$$

The estimated entropies are given in Table III. Once the Gibbs energies and entropies of ions are known at

(30) Peterson, J. H. U.S. Patent No. 2,216,655, Oct 1940.
(31) Christensen, A. N.; Rasmussen, S. E. *Acta Chem. Scand.* **1963**, *17*, 845.
(32) Vivekanandan, R.; Philip, S.; Kutty, T. R. N. *Mater. Res. Bull.* **1986**, *22*, 99.
(33) Kutty, T. R. N.; Vivekanandan, R.; Murugaraj, P. *Mater. Chem. Phys.* **1988**, *19*, 533.
(34) Uedaira, S.; Yamanoi, H.; Tamura, H. U.S. Patent No. 4,520,004, May 1985.
(35) Lilley, E.; Wusirika, R. R. Eur. Pat. Appl. EP 0 250 085 A2, Published Dec 1987.
(36) Anger, J.-F. Unpublished data.
(37) Naumov, G. B.; Ryzhenko, B. N.; Khodakovsky, I. L. *Handbook of Thermodynamic Data*; Barnes, I., Speltz, V., Eds.; U.S. Geological Survey, 1974.
(38) Chen, C. M.; Aral, K.; Theus, G. *Computer-Calculated Potential pH Diagrams to 300 °C, Handbook of Diagrams*; EPRI in association with Babcock & Wilcox Company: Alliance, OH, 1983; Vol. 2.
(39) Baes, Ch F., Jr.; Mesmer, R. E. *Am. J. Sci.* **1981**, *281*, 935.
(40) Barner, H. E.; Scheuerman, R. V. *Handbook of Thermochemical Data for Compounds and Aqueous Species*; Wiley-Interscience: New York, 1978.
(41) Kubaschewski, O.; Evans, E. Ll. *Metallurgical Thermochemistry*, 3rd ed.; Pergamon Press: New York, 1958.
(42) Barin, I.; Knacke, O.; Kubaschewski, O. *Thermochemical Properties of Inorganic Substances*; Springer-Verlag:Berlin, 1973 and 1977, supplement.
(43) *Chemical Engineer's Handbook*, 5th ed.; Perry, J. H., Chilton, C. H., Kirkpatrick, S. D., Eds.; McGraw-Hill: New York, 1973.
(44) Robie, R. A.; Hemingway, B. S.; Fisher, J. R. U.S. Geological Survey Bulletin 1452; U.S. Government Printing Office: Washington, DC, 1979.
(45) Lange, N. A. *Lange's Handbook of Chemistry*, 11th ed.; Dean, J. A., Ed.; McGraw-Hill: New York, 1973.
(46) Baes, Ch. F., Jr.; Mesmer, R. E. *The Hydrolysis of Cations*; Wiley-Interscience: New York, 1976.
(47) Reid, R. C.; Prausnitz, J. M.; Poling, B. E. *The Properties of Gases and Liquids*, 4th ed.; McGraw-Hill: New York, 1987.
(48) Powell, R. E.; Latimer, W. M. *J. Chem. Phys.* **1951**, *19*, 1139.
(49) Sverjensky, D. A. *Rev. Miner.* **1987**, *17*, 177.
(50) Watson, D. J.; Randall, C. A.; Newnham, R. E.; Adair, J. H. *Ceramic Transactions, Ceramic Powder Science IIA*; Messing, G. L., Fuller Jr., E. R., Hausner, H., Eds.; American Ceramic Society: Westerville, OH, 1988; Vol. 1, p 154.
(51) Kutty, T. R. N.; Balachandran, R. *Mater. Res. Bull.* **1984**, *29*, 1479.
(52) Kaneko, S.; Imoto, F. *Bull. Chem. Soc. Jpn.* **1978**, *51*, 1739.
(53) Suzuki, M.; Uedaira, S.; Masuya, H.; Tamura, H. *Ceramic Transactions, Ceramic Powder Science IIA*; Messing, G. L., Fuller Jr., E. R., Hausner, H., Eds.; American Ceramic Society: Westerville, OH, 1988; Vol. 1, p 163.
(54) Rosetti, G. A.; Watson, D. J., Jr.; Newnham, R. E.; Adair, J. H. *J. Cryst. Growth* **1992**, *116*, 251.
(55) Takai, K.; Shoji, S.; Naito, H.; Sawaoka, A. *Proceedings of the First International Symposium on Hydrothermal Reactions*; Somiya, S., Ed.; Gakujutsu Bunken Fukyu-Kai: Tokyo, Japan, 1982; p 877.
(56) Fox, G. R.; Adair, J. H.; Newnham, R. E. *J. Mater. Sci.* **1991**, *26*, 1187.
(57) Robinson, R. A.; Stockes, R. H. *Electrolyte Solutions*, 2nd ed.; Butterworth: London, 1965.

Table III. Relevant Species in the Ba–Ti and Pb–Ti Hydrothermal Systems and Their Standard State Properties at 298.15 K

	ionic species				
	H^+	$BaOH^+$	$BaHCO_3^+$	Ba^{2+}	Ti^{4+}
$\Delta G°_f$/(kJ mol^{-1})	0	−716.72	−1153.5	−560.78	−354.18
$\Delta H°_f$/(kJ mol^{-1})	0	−749.35	−1207.2	−537.64	
$S°$/(J mol^{-1} K^{-1})	0	55.5	195.9	9.62	−456.5
$C°_p$/(J mol^{-1} K^{-1})	0	44.0		−12.3	
$10^6\,V°$/(m^3 mol^{-1})	0			−12.6	
lit.		14, 21	16	16, 21	14, 21

	ionic species				
	$TiOH^{3+}$	$Ti(OH)_2^{2+}$	$Ti(OH)_3^+$	Pb^{2+}	$PbOH^+$
$\Delta G°_f$/(kJ mol^{-1})	−614.00	−869.56	−1092.5	−23.89	−217.74
$\Delta H°_f$/(kJ mol^{-1})				0.920	−224.48
$S°$/(J mol^{-1} K^{-1})	−189.5	−40.8	56.9	17.6	146.4
$C°_p$/(J mol^{-1} K^{-1})				−53.1	−11.21
$10^6\,V°$/(m^3 mol^{-1})				−65.3	
lit.	14, 39	14, 39	14, 39	16, 21	16, 21, 49

	ionic species				
	Pb_2OH^{3+}	$Pb_3(OH)_4^{2+}$	$Pb_4(OH)_4^{4+}$	$Pb_6(OH)_8^{4+}$	OH^-
$\Delta G°_f$/(kJ mol^{-1})	−248.72	−888.68	−936.38	−1800.4	−157.30
$\Delta H°_f$/(kJ mol^{-1})		−1038.1	−1066.1	−1090.3	−230.03
$S°$/(J mol^{-1} K^{-1})	104.6	192.5	150.6	414.2	−10.7
$C°_p$/(J mol^{-1} K^{-1})					
$10^6 V°$/(m^3 mol^{-1})					
lit.	46, 48	40	40	40	11

	ionic species			
	CO_3^{2-}	HCO_3^-	$HTiO_3^-$	$HPbO_2^-$
$\Delta G°_f$/(kJ mol^{-1})	−527.98	−586.94	−955.88	−338.75
$\Delta H°_f$/(kJ mol^{-1})	−675.23	−689.93		−431.19
$S°$/(J mol^{-1} K^{-1})	−50.0	98.4	117.3	92.0
$C°_p$/(J mol^{-1} K^{-1})	−290.8	−35.4		
$10^6 V°$/(m^3 mol^{-1})	−21.0	102.9		
lit.	16, 21	16, 21	38	16, 21

	aqueous species				
	H_2O	$Ti(OH)_4$	CO_2	$BaCO_3$	PbO
$\Delta G°_f$/(kJ mol^{-1})	−237.25	−1318.38	−385.97	−1103.9	−164.08
$\Delta H°_f$/(kJ mol^{-1})	−285.83	−1511.26	−413.80	−1196.0	−187.03
$S°$/(J mol^{-1} K^{-1})	70.0	54.8	117.6	66.9	92.0
$C°_p$(J mol^{-1} K^{-1})	75.3	50.2	243.1		
lit.	11	14	16, 22	16	16

	solid species				
	$Ba(OH)_2$	$BaCO_3$	$BaTiO_3$	BaO	$Ba(OH)_2{\cdot}8H_2O$
$\Delta G°_f$/(kJ mol^{-1})	−855.17	−1164.8	−1572.4	−525.35	−2779.9
$\Delta H°_f$/(kJ mol^{-1})	−941.40	−1244.7	−1659.8	−553.54	−3328.4
$S°$/(J mol^{-1} K^{-1})	108.8	112.1	107.9	70.4	422.6
$C°_p$/(J mol^{-1} K^{-1})[a]	97.9		102.5		
a/(J mol^{-1} K^{-1})	116.8	89.96	121.5	53.30	
$10^3 b$/(J mol^{-1} K^{-2})	18.44	46.28	8.535	4.351	
$10^{-5} c$/(J mol^{-1} K)	−18.41	−16.36	19.16	8.301	
$10^6 V°$/(m^3 mol^{-1})	38.19	45.81	38.80	25.59	144.7
lit.	14, 13b, 43	16	15, 41, 37	15, 41, 44	14, 45

	solid species					
	Ba_2TiO_4	TiO_2 (rutile)	TiO_2 (anatase)	PbO (litharge)	PbO (massicot)	$PbTiO_3$
$\Delta G°_f$/(kJ mol^{-1})	−2132.9	−890.70	−883.27	−189.28	−188.65	−1111.9
$\Delta H°_f$/(kJ mol^{-1})	−2243.0	−946.01	−938.72	−219.40	−218.06	−1198.7
$S°$/(J mol^{-1} K^{-1})	196.6	50.3	49.9	66.3	68.7	111.9
$C°_p$/(J mol^{-1} K^{-1})[a]	152.6	55.1	55.3	45.8	47.8	104.4
a/(J mol^{-1} K^{-1})	179.9	62.82	75.04	46.36	37.87	119.5
$10^3 b$/(J mol^{-1} K^{-2})	6.694	11.38	0.0	11.34	26.78	17.91
$10^{-5} c$/(J mol^{-1} K)	−29.12	−9.897	−17.63	−3.556	0.0	−18.20
$10^6 V°$/(m^3 mol^{-1})		18.82	20.52	23.91	23.15	
lit.	15, 41	16	15, 42, 44	15, 37, 44	15, 41, 44	15, 42

[a] Heat capacities are calculated from the relation $C°_p = a + bT + cT^{-2}$.

298.15 K, their values at other temperatures and pressures can be calculated from the method of Helgeson et al.[20,21,16]

The standard-state properties described above were used to construct stability diagrams for the Ba–Ti system. The

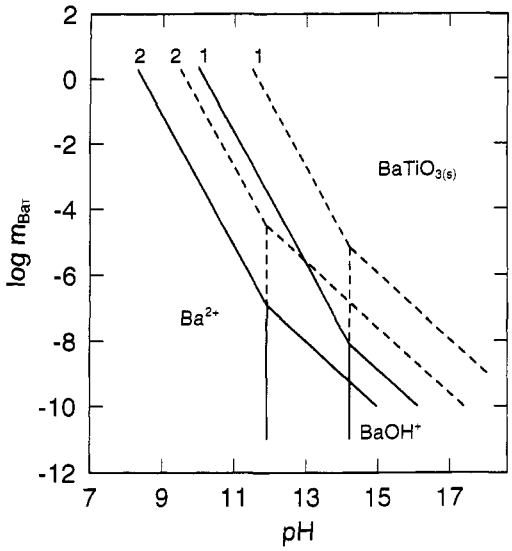

Figure 1. Calculated stability diagram for the Ba–Ti hydrothermal system using an ideal-solution approximation at 298.15 (1) and 363.15 K (2). The solid and dashed lines denote the results obtained using the data of Barin[15] and Naumov et al.,[37] respectively.

calculated stability diagrams show which species predominate at a given T, pH and total concentration of either Ba (m_{Ba_T}) or Ti (m_{Ti_T}). In all cases, autogenous pressure was assumed.

The stability diagrams were obtained by solving the equilibrium and balance equations for different input compositions to cover the whole m_{Ba_T} vs pH or m_{Ti_T} vs pH plane. Calculations were performed at T = 298.15 K and 363.15 K. The latter temperature has been empirically found to be appropriate for the hydrothermal synthesis of $BaTiO_3$(s).[32,36]

Figure 1 shows the stability diagrams calculated at 298.15 K (lines 1) and 363.15 K (lines 2) using ideal solution approximation (i.e., with all activity coefficients assumed to be equal to one). These diagrams have been obtained using two standard-state property data sets reported for $BaTiO_3$(s) by Barin[15] and Naumov et al.[37] Thus, this figure illustrates the effect of deviation in standard state properties on stability diagrams. As shown in Figure 1, the differences between standard state data can shift the boundaries between phase stability regions by as much as 1–1.5 pH units. As explained above, the data of Barin[16] are deemed more reliable and have been, therefore, used for all remaining calculations reported in this work.

Figures 2 and 3 show the results obtained using the complete thermodynamic model at 298.15 and 363.15 K, respectively (solid lines). For comparison, the results obtained using the ideal-solution approximation are shown as dashed lines. In both cases, the boundaries are shown between aqueous Ba^{2+} and solid $BaTiO_3$(s), aqueous Ba^{2+} and $BaOH^+$, and aqueous $BaOH^+$ and solid $BaTiO_3$(s). As evident from Figures 2 and 3, the phase boundaries calculated from the complete and simplified (ideal solution) models are markedly different. In contrast to the ideal-solution case, the phase boundaries calculated from the complete model are no longer represented by straight lines. Their curvature is especially significant for higher concentrations of aqueous species ($m_{Ba_T} > 10^{-4}$). When solution nonideality is introduced, the phase boundaries are shifted toward higher pH values. The Ba^{2+}–$BaOH^+$ boundary is shifted by ca. 2 pH units whereas the

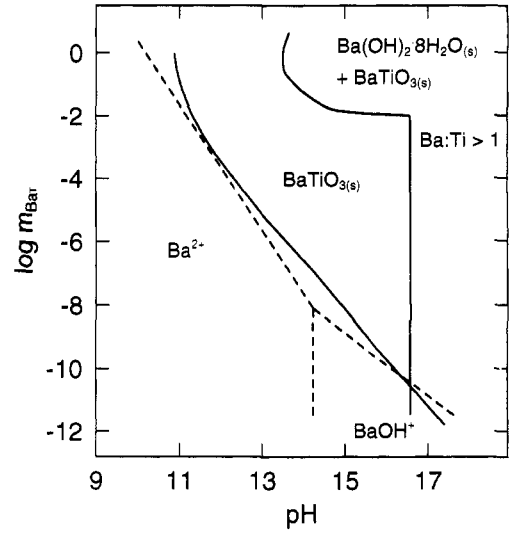

Figure 2. Calculated stability diagram for the Ba–Ti system at 298.15 K using modeled activity coefficients. Standard-state data were taken from the compilation of Barin.[15] For comparison, the ideal-solution results are shown as dashed lines.

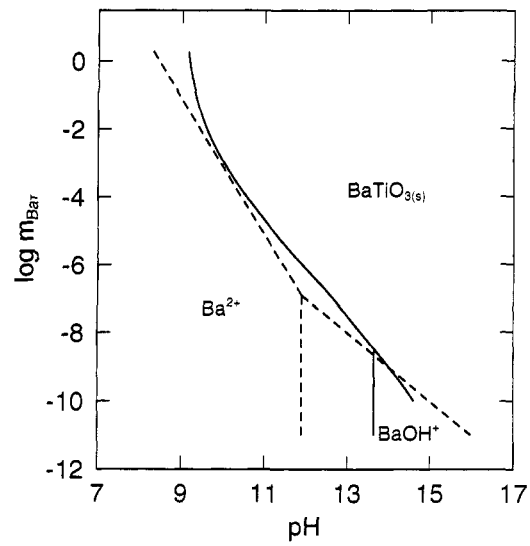

Figure 3. Calculated stability diagram for the Ba–Ti system at 363.15 K using modeled activity coefficients. Standard state data were taken from the compilation of Barin.[15] For comparison, the ideal-solution results are shown as dashed lines.

Ba^{2+}–$BaTiO_3$(s) boundary is shifted by ca. 1 unit at both temperatures. The predominance field of $BaOH^+$ ions predicted using modeled activity coefficients is much smaller than that estimated using the ideal solution approximation and appears at lower total concentrations of Ba.

It is evident from Figures 2 and 3 that solution nonideality has an important effect on the location of phase boundaries. The simplified ideal-solution model leads to significant deviations from the results of more rigorous calculations. The magnitude of solution nonideality is additionally illustrated in Table IV which shows the activity coefficients of aqueous species in equilibrium with solid $BaTiO_3$(s).

The stability diagrams (Figures 2 and 3) illustrate the effect of process variables such as m_{Ba_T}, pH, T, and the Ba/Ti ratio on the synthesis of barium titanate $BaTiO_3$(s).

$BaTiO_3$(s) can be obtained in the whole range of m_{Ba_T} provided that pH is appropriately chosen. The higher is

Table IV. Activity Coefficients of Aqueous Species in Equilibrium with $BaTiO_3$(s) at 363.15 K

	m_{Ba_T}/mol kg^{-1}; I^a/mol kg^{-1}		
	10^{-5}; 0.0789	0.0017; 0.0050	1.0000; 2.8800
$\gamma_{Ba^{2+}}$	0.3291	0.7038	0.0362
γ_{BaOH^+}	0.7651	0.9164	0.5718
γ_{H^+}	0.7454	0.9153	0.5417
γ_{Na^+}	0.7654	0.9164	0.4492
$\gamma_{Ti^{4+}}$	0.0227	0.2525	0.00001
$\gamma_{TiOH^{3+}}$	0.0648	0.4489	0.0005
$\gamma_{Ti(OH)_2^{2+}}$	0.3557	0.7063	0.0343
$\gamma_{Ti(OH)_3^+}$	0.7666	0.9165	0.4304
$\gamma_{HTiO_3^-}$	0.7454	0.9182	0.8423
γ_{OH^-}	0.7654	0.9166	0.5166
$\gamma_{Ti(OH)_4(aq)}$	1.0230	1.0010	1.1200

[a] I: ionic strength.

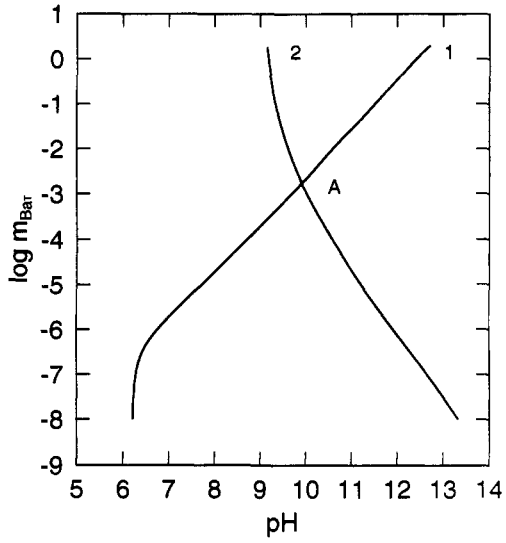

Figure 4. Comparison of the pH of a $Ba(OH)_2$(s) solution (curve 1) with the pH that is necessary to precipitate $BaTiO_3$(s) from the solution (curve 2).

the total concentration of Ba in solution (m_{Ba_T}), the lower can be the pH to cause the precipitation of $BaTiO_3$(s). For example, pH that is necessary to precipitate $BaTiO_3$(s) from a 1 m solution of barium is 9.2 at T = 363.15 K; it increases to 11.2 for a 10^{-5} m solution of barium.

Barium hydroxide ($Ba(OH)_2$(s)) is the most obvious feedstock, along with titanium dioxide (TiO_2(s)), to synthesize barium titanate ($BaTiO_3$(s)). However, an aqueous solution of $Ba(OH)_2$(s) may not be sufficiently alkaline for the synthesis of $BaTiO_3$(s). This is shown in Figure 4 which compares the pH of an aqueous solution of $Ba(OH)_2$(s) (curve 1) with the pH that is necessary to initiate the formation of $BaTiO_3$(s) (curve 2). If m_{Ba_T} is greater than 0.0017 (point A), the alkalinity of a $Ba(OH)_2$(s) solution is sufficient for the precipitation of $BaTiO_3$(s). For lower values of m_{Ba_T}, additional mineralizers, such as NaOH or KOH should be introduced. For this case, Figure 5 shows the ratios of molalities of NaOH to m_{Ba_T} that has to be maintained in order to initiate the precipitation of $BaTiO_3$(s) for $m_{Ba_T} \leq 0.0017$ (curve 1) or to obtain 99.995% of the precipitate (curve 2).

The formation of $BaTiO_3$(s) consumes equimolar amounts of Ba and Ti (Ba/Ti = 1, Table II, reaction 6). If different relative amounts of Ba and Ti are used (Ba/Ti $\neq$ 1), the location of phase boundaries does not change. However, the Ba/Ti ratio may have an important effect on the synthesis. Notably, an excess amount of Ti (Ba/Ti < 1) will cause a contamination of $BaTiO_3$(s) with TiO_2-

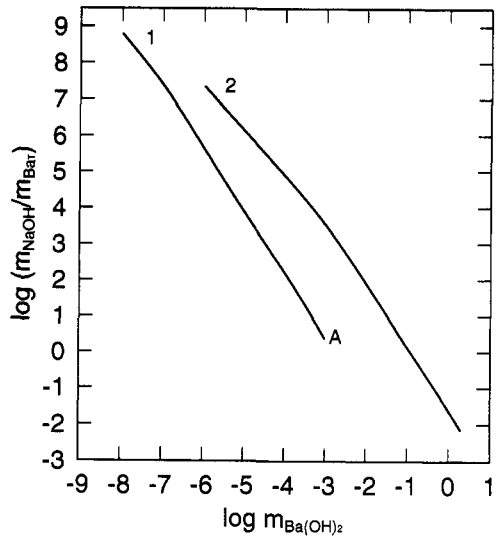

Figure 5. Ratio of molality of NaOH to m_{Ba_T} that is necessary to initiate the precipitation of $BaTiO_3$(s) for $m_{Ba_T} < 0.0017$ (curve 1) and to obtain 99.995% of the precipitate (curve 2).

(s), which is stable under hydrothermal conditions. Moderate excess amounts of barium (Ba/Ti > 1) will increase, on the other hand, the pH of the solution. This is desirable for the hydrothermal synthesis as it makes it possible to avoid the use of an alkaline mineralizer (e.g., NaOH). The amount of excess Ba required to ensure a complete reaction is a function of the concentration of the reagents employed. For example, when a 0.01 m $Ba(OH)_2$(s) solution is used a Ba/Ti ratio equal to 1.167 is required to ensure 99.995% complete reaction. In contrast, when 2 m $Ba(OH)_2$(s) solution is used the Ba/Ti ratio can be reduced to 1.001.

However, excessive amounts of barium may cause the precipitation of other, undesirable species. In particular, the hydrate $Ba(OH)_2 \cdot 8H_2O$(s) will precipitate at 298.15 K for pH > 13.58 and $m_{Ba_T} \geq 10^{-2}$ and for pH > 16.50 and $m_{Ba_T} < 10^{-2}$. The threshold temperature below which the hydrate precipitates is 338 K. This result has important practical implications as it indicates that the obtained $BaTiO_3$(s) powder can be contaminated with $Ba(OH)_2 \cdot 8H_2O$(s) below 338 K.

The stability diagrams are also affected by temperature. The phase boundaries are shifted toward lower pH values with an increase in temperature. Also, temperature determines the appearance or disappearance of additional solid species (e.g., $Ba(OH)_2 \cdot 8H_2O$(s)). In comparison with temperature, pressure has a minor effect because all reactions involved in the synthesis proceed in a condensed phase with limited compressibility.

Additionally, Figures 6 and 7 show the distribution and the stability diagram of titanium species in the Ba–Ti system as a function of the solution pH at 298.15 K, respectively. As shown in Figure 6, $Ti(OH)_2^{2+}$ is the predominant species for pH < 2.45 whereas $Ti(OH)_4$(aq) is predominant for pH > 2.45. Also, $TiOH_3^+$ occurs in significant, although smaller, quantities for 1 < pH < 4.6. For the conditions of practical hydrothermal synthesis (i.e., pH > 9 and $m_{Ti_T} > 10^{-5}$), TiO_2(s) is stable. This confirms that the ratio Ba/Ti should not be smaller than one to avoid the contamination of $BaTiO_3$(s) with the remaining TiO_2(s).

Effect of CO_2(g) on the Synthesis of $BaTiO_3$(s). The proposed method makes it possible to analyze the effect of CO_2(g) on the hydrothermal synthesis. Carbon dioxide

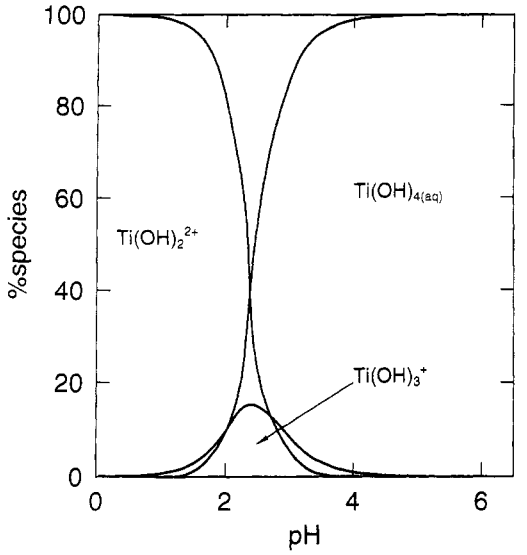

Figure 6. Distribution of various aqueous Ti species in the Ba–Ti system as a function of pH at 298.15 K.

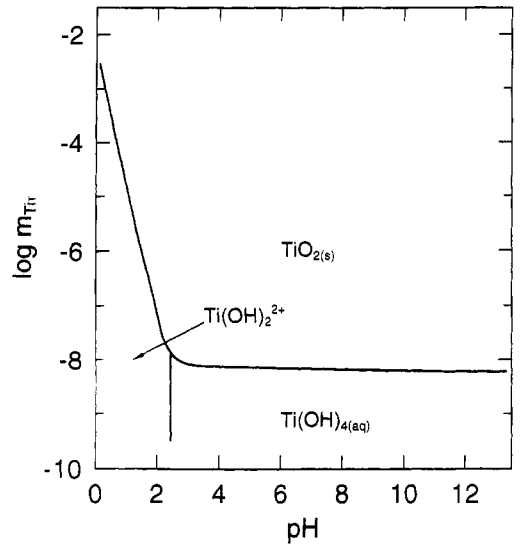

Figure 7. Calculated stability diagram of aqueous Ti species at 298.15 K using modeled activity coefficients.

acts as a contaminant because of its appreciable concentration in the atmosphere. Standard state data for $BaCO_3$(s), $BaCO_3$(aq), CO_2(aq), $BaHCO_3^+$, HCO_3^-, CO_3^{2-}, H_2O(g), and CO_2(g) have been taken from Johnson et al.[16] and CODATA.[11] Fugacity coefficients of gaseous species were estimated using the critical parameters from Reid et al.[47]

Calculations have been performed for two cases: (1) assuming that a constant partial pressure of CO_2(g) (33.54 Pa) is maintained over the hydrothermal solution which corresponds to an open system with respect to CO_2(g) and (2) assuming that the reaction proceeds in a closed autoclave with about 20% of its volume filled with air containing atmospheric carbon dioxide, this case simulates the real conditions of a hydrothermal experiment.

The results obtained in case 1 are shown in Figure 8. In an open system with respect to CO_2(g), the desirable $BaTiO_3$(s) does not form at all because $BaCO_3$(s) is inherently more stable. In the closed system, which drastically reduces the availability of CO_2(g), $BaCO_3$(s) tends to precipitate at concentrations of Ba higher than ca. 10^{-5} m (Figure 9). $BaCO_3$(s) precipitates at lower pH values than those needed to precipitate $BaTiO_3$(s). Therefore, the precipitated $BaTiO_3$(s) will be always contaminated with some amount of $BaCO_3$(s) if the solution is concentrated with respect to Ba (i.e., if $m_{Ba_T} > 10^{-5}$). This suggests that the exposure to CO_2(g) should be always avoided while synthesizing $BaTiO_3$(s).

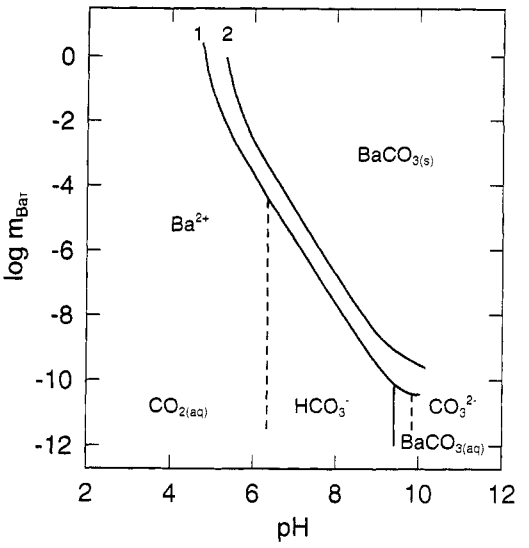

Figure 8. Calculated stability diagram for the Ba–Ti system under air corresponding to a fixed partial pressure of CO_2(g) (p_{CO_2}(g) = 33.54 Pa) at 298.15 (1) and 363.15 K (2).

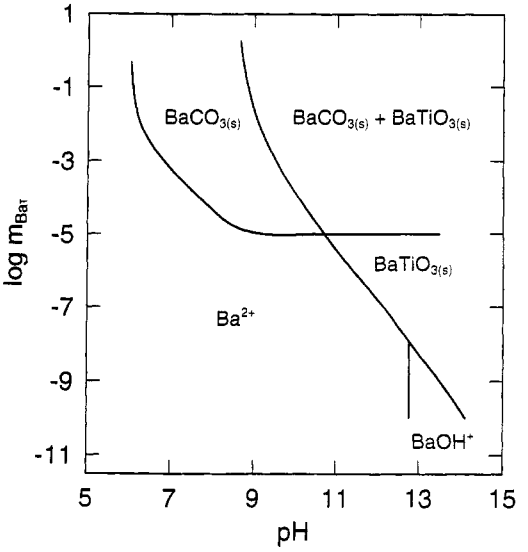

Figure 9. Calculated stability diagram for the Ba–Ti system in a sealed vessel containing 20 vol. % air (CO_2(g)-containing) at 363.15 K.

Synthesis of $PbTiO_3$(s). For simulating the hydrothermal synthesis of $PbTiO_3$(s), the standard state data for PbO(s) (both massicot and litharge) and $PbTiO_3$(s) were taken from Barin's compilation.[15] Data for $Pb(OH)_2$(s) were taken from Medvedev et al.[14] For the common aqueous species PbO(aq), Pb^{2+}, $PbOH^+$, and $HPbO_2^-$, the data from Johnson et al.[16] were used. For the less common species Pb_2OH^{3+}, $Pb_3(OH)_4^{2+}$, and $Pb_4(OH)_4^{4+}$, and $Pb_6(OH)_8^{4+}$, which are absent in the above sources, the data from Barner and Scheuerman[40] and Baes and Mesmer[46] were adopted. The standard state data are listed in Table III. It was found that the results were not sensitive to choosing either massicot or litharge.

The results of calculations are shown in Figure 10 for T = 325.15 K and in Figure 11 for T = 373.15 K. Additionally, Figure 12 shows the distribution of lead

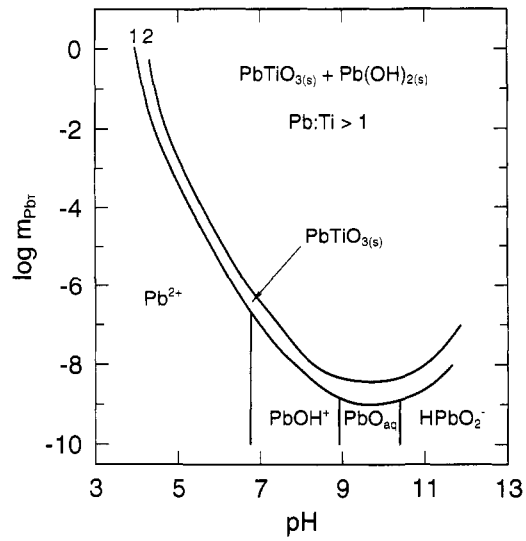

Figure 10. Calculated stability diagram for the aqueous Pb–Ti system at 323.15 K.

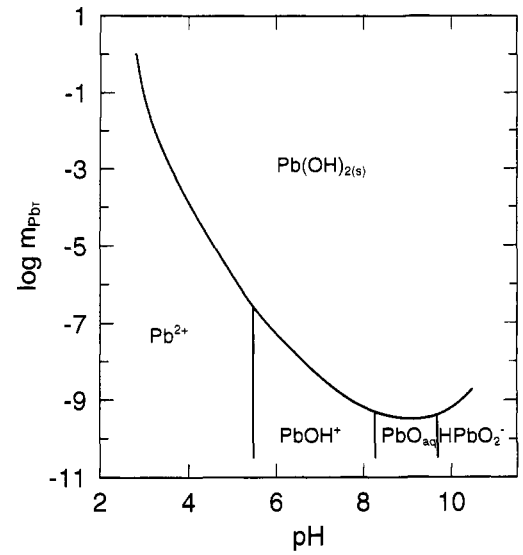

Figure 11. Calculated stability diagram for the aqueous Pb–Ti system at 373.15 K.

species in the hydrothermal Pb–Ti system as a function of pH at 323.15 K.

The most important feature of the Pb–Ti hydrothermal system is the competition between the precipitation of lead titanate ($PbTiO_3$(s)) and lead hydroxide ($Pb(OH)_2$(s)). Figure 10 shows solubility curves for $PbTiO_3$(s) (curve 1) and $Pb(OH)_2$(s) (curve 2) at 323.15 K. Both curves have a similar shape and show a minimum at $9.5 < pH < 9.7$. The distance between the curves is ca. 0.3–0.5 pH units and remains the same in the entire concentration range. Similarly as in the case of $BaTiO_3$(s), the synthesis of $PbTiO_3$(s) consumes equimolar amounts of Pb and Ti (Table II, reaction 30) and, therefore, phase pure perovskite will be obtained when the ratio Pb/Ti is equal to one. Any excess amount of Pb will cause precipitation of $Pb(OH)_2$(s). The effect of temperature on the solubility curves is similar as in the case of the Ba–Ti system, i.e., the solubility of $PbTiO_3$(s) and $Pb(OH)_2$(s) phase field shifts toward lower pH with an increase in temperature while $PbTiO_3$(s) phase field disappears. Thus, a temperature ($T \cong 348$ K) exists for which $PbTiO_3$(s) and $Pb(OH)_2$(s) can coprecipitate. At temperatures below 348 K, $PbTiO_3$(s) is more stable and the precipitation of $Pb(OH)_2$(s) can be

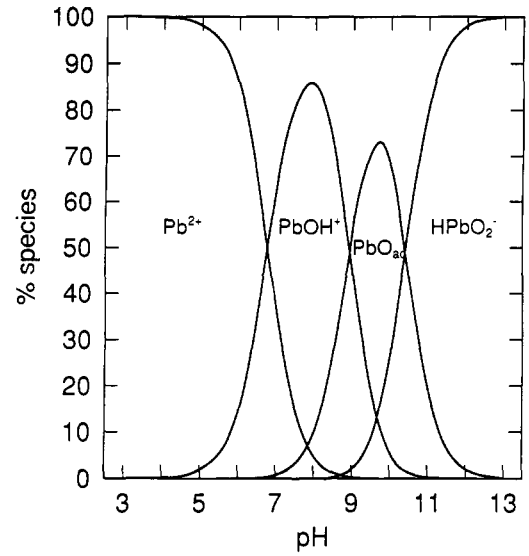

Figure 12. Distribution of aqueous Pb species in the Pb–Ti system as a function of pH at 323.15 K.

avoided if no excess amount of Pb is present over that required to produce stoichiometric lead titanate ($PbTiO_3$(s)). This suggests a possible low-temperature synthesis route to obtain $PbTiO_3$(s). At 373.15 K (Figure 11), $Pb(OH)_2$(s) is more stable and precipitates, thus consuming all available Pb and making it impossible to precipitate $PbTiO_3$(s).

Comparison of calculated diagrams with reported $PbTiO_3$(s) syntheses is supportive. Fox et al.[8,56] obtained a $PbTiO_3$(s) precursor powder by coprecipitation from a mixed solution of $TiCl_4$(aq) and $Pb(NO_3)_2$(s) at 318.15 K, which was assumed to be an amorphous $PbTiO_3$(s) powder. Unfortunately, most of the literature is irrelevant since temperatures greater than ca. 433 K were employed to obtain crystalline $PbTiO_3$(s).[50–55]

In this study we explored a low-temperature route to the synthesis of $PbTiO_3$(s) using lead oxide PbO(s) and titanium dioxide TiO_2(s) as feedstocks. It should be noted that the activity coefficient model and standard state data are most accurate at low and moderate temperatures and lose accuracy above ca. 473 K. Therefore, the predictive technique proposed in this work seems to be most appropriate for low-temperature synthesis.

The obtained results suggest that such synthesis is possible and warrants further experimental investigation. In a forthcoming work we will focus on determining the optimum feedstocks and conditions for this synthesis.

Conclusions

The above results show that phase stability diagrams can be rigorously generated for hydrothermal systems of ceramic interest. As demonstrated for $BaTiO_3$(s), the use of reliable standard state thermodynamic data is crucial for the calculations. A careful critical evaluation of the data is necessary for each case. The obtained results demonstrate that the effect of solution nonideality on hydrothermal reactions is very significant. PH is an important thermodynamic variable for the synthesis of perovskite materials. Both $PbTiO_3$(s) and $BaTiO_3$(s) stability exhibit a strong dependency on solution pH and total concentration on Ba (m_{Ba_T}) or Pb (m_{Pb_T}) species. In addition, pH and total concentration of Ba and Pb must be monitored to avoid the precipitation of impurity

hydroxide phases. Tailoring the pH and m_{Ba_T} to obtain phase pure powders may require either addition of a mineralizer (e.g., NaOH) or maintaining Ba/Ti ratios greater than 1. In contrast, for the lead system, Pb/Ti ratio greater than 1 can lead to impurity phases unless a temperature of 348 K or less is maintained. The effect of temperature on either $BaTiO_3$(s) or $PbTiO_3$(s) shifts the solubility curves to lower pH values. Finally, for $BaTiO_3$(s), carbon dioxide exposure should be avoided since it leads toward the precipitation of a $BaCO_3$(s) impurity phase.

Acknowledgment. We gratefully acknowledge the generous support of the Materials Division (Code 1131) at the Office of Naval Research (ONR) under the auspices of the ONR Young Investigator Program. We would also like to acknowledge the scientists at OLI Systems, Inc. for their helpful technical input.